Enhanced Second-Order Nonlinearity for THz Generation by Resonant Interaction of Exciton-Polariton Rabi Oscillations with Optical Phonons

Katharina Rojan,[1,2] Yoan Léger,[3] Giovanna Morigi,[2] Maxime Richard,[4] and Anna Minguzzi[1,*]
[1]Univ. Grenoble Alpes, CNRS, LPMMC, 38000 Grenoble, France
[2]Theoretische Physik, Universität des Saarlandes, D-66123 Saarbrücken, Germany
[3]UMR FOTON, CNRS, INSA, F-35708 Rennes, France
[4]Univ. Grenoble Alpes, CNRS, Grenoble INP (Institute of Engineering Univ. Grenoble Alpes), Institut Néel, 38000 Grenoble, France
(Received 12 June 2017; published 18 September 2017)

Semiconductor microcavities in the strong-coupling regime exhibit an energy scale in the terahertz (THz) frequency range, which is fixed by the Rabi splitting between the upper and lower exciton-polariton states. While this range can be tuned by several orders of magnitude using different excitonic media, the transition between both polaritonic states is dipole forbidden. In this work, we show that, in cadmium telluride microcavities, the Rabi-oscillation-driven THz radiation is actually active without the need for any change in the microcavity design. This feature results from the unique resonance condition which is achieved between the Rabi splitting and the phonon-polariton states and leads to a giant enhancement of the second-order nonlinearity.

DOI: 10.1103/PhysRevLett.119.127401

A room temperature compact solid-state terahertz (THz) source is a highly desirable piece of equipment, needed in many domains like communication, health, or security [1]. Different semiconductor-based techniques already exist, based on cascade laser structures, optical nonlinearity, or photomixing in electronic structures, but so far they all require advanced cooling techniques [2,3].

Although coincidental, it turns out that semiconductor microcavities in the strong-coupling regime [4] exhibit the right energy scale for THz electromagnetic radiation. Indeed, the normal mode (Rabi) splitting, i.e., the energy splitting between the upper and lower exciton-polariton states resulting from the strong-coupling regime, typically ranges from 3.5 meV (i.e., 0.85 THz) in GaAs microcavities to hundreds of meV (i.e., tens of THz) in large band gap semiconductor systems. And yet, such a transition cannot be used directly to generate or absorb THz photons, as it features no dipole moment.

To circumvent this problem, several strategies have been proposed. In a pioneering experiment, an in-plane static electric field was used to hybridize excitonic states with different parities (i.e., s-like and p-like) resulting in a nonzero dipole moment between the upper and lower polariton branches [5]. More recently, taking advantage of the bosonic nature of polaritons, it has been proposed to optically excite p-like excitons by two-photon absorption and to achieve bright THz emission by stimulated relaxation toward the lower polariton branch [6,7]. However, due to ultrafast relaxation of the p excitons, this mechanism has remained elusive so far [8]. Other promising ideas have been put forward, e.g., intersubband polariton microcavities involving doped asymmetrical quantum wells [9], phonon-polariton propagation in suspended waveguides [10], or microcavities embedding a $\chi^{(2)}$ active material like [111]-oriented GaAs [11].

The common point in these proposals is to modify the microcavity structure, either by applying an external field or by engineering the material, in order to build up a $\chi^{(2)}$ optical nonlinearity resonant with the polariton states and to use it for frequency difference generation. In this work, we show that a threefold-resonant condition can be reached when the Rabi splitting is tuned at resonance with a mechanical vibration mode related to the lattice unit-cell deformation, i.e., the transverse-optical (TO) phonon. This mechanism does not require any externally applied field or any new materials.

The most extensively used material to fabricate microcavities in the strong-coupling regime is gallium arsenide [12]. In this material, this resonance condition is hard to meet, as the typical achievable Rabi splitting is, in general, much smaller than the TO phonon energy ($\hbar\omega_{\mathrm{TO}}=33.3\,\mathrm{meV}$). A CdTe-based microcavity will be considered in this Letter as such microcavities exhibit a near perfect match between the typical microcavity Rabi splitting [13] and the TO phonon energy $\hbar\omega_{\mathrm{TO}} = 18$ meV, with the additional benefit of a much better thermal stability tested up to $T = 200$ K [14].

Our proposal relies on a cascade of three different mechanisms already present in current state-of-the art microcavities, namely, (i) the strong-coupling regime between optical cavity photons and excitons, (ii) the strong-coupling regime between THz photons and TO phonons (i.e., the so-called phonon-polariton states which are intrinsic to most semiconductor materials, including the ones cited in this Letter) [15], and (iii) the deformation-potential-mediated interaction between the exciton hole and the TO phonons. The latter provides the effective $\chi^{(2)}$ nonlinearity enabling the conversion of the laser-pumped upper and lower

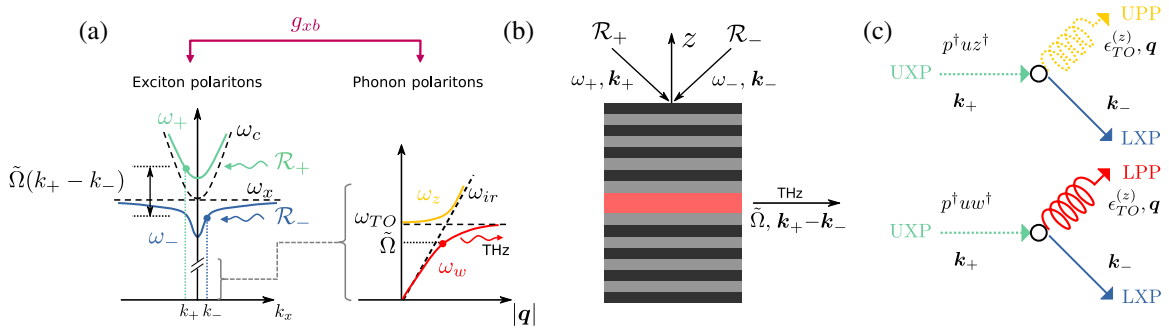

FIG. 1. (a) Sketch of the conversion mechanism: Left, upper (green curve, ω_+) and lower (blue curve, ω_-) exciton-polariton dispersion branches along the x axis; right, upper (yellow curve, ω_z) and lower (red curve, ω_W) phonon-polariton branches vs wave vector $|\boldsymbol{q}|$. Dots in exciton-polariton branches indicate an example of laser-pumped states with intensity $\mathcal{R}_+$ and $\mathcal{R}_-$, respectively, with frequency difference $\tilde{\Omega}$. The dot in the lower phonon-polariton branch shows the state emitting THz radiation at frequency $\tilde{\Omega}/2\pi$. (b) Pump scheme: The excitation laser beams impinges the cavity surface each with an angle such that $\sin(\theta_\pm) = ck_\pm/\omega_\pm$. The generated phonon polaritons propagate in the cavity plane with $\boldsymbol{q} = \boldsymbol{k}_+ - \boldsymbol{k}_-$ and decay at the interface into THz radiation. (c) Elementary interaction mechanisms: An upper exciton polariton (UXP) is annihilated to create a lower exciton polariton (LXP) plus a phonon polariton (upper or lower depending on $\tilde{\Omega}$).

exciton-polariton field into THz photons. We focus on TO phonons, because, although longitudinal optical (LO) phonons are much better coupled to excitons via the Frölich mechanism, they are not coupled to THz photons and are thus useless in our scheme. Interestingly, (iii) is formally the same interaction mechanism that appears in the context of optomechanics, except that photons are replaced by excitons and that both oscillators benefit from a continuum spectrum of phononic excitations. Frequency conversion schemes in the microwave domain have indeed been achieved by purely optomechanical means using high-Q mechanical resonators [16–18]. In our case, mechanical vibrations are also at the heart of the mechanism, as TO phonons correspond to the mechanical deformation of the few-angstrom-sized crystal unit cell.

A detailed physical picture of our conversion scheme is sketched in Fig. 1(a): By optically exciting simultaneously both upper and lower polaritons, an excitonic density is created in the microcavity active region (a slab of bulk semiconductor), which is time modulated at the Rabi frequency. This population beat induces mechanical vibration within the active region via a deformation-potential interaction. In our scheme, this modulation frequency matches that of a TO-phonon-polariton state, so that the earlier excites the latter. Finally, the resulting phonon polaritons propagate in the structure and decay radiatively into THz photons upon reaching an interface or by interacting with a structured dielectric environment.

Accounting for this cascade of interactions, the system's Hamiltonian consists of four terms:

$$\hat{\mathcal{H}} = \hat{\mathcal{H}}_{\text{exc-cavity}} + \hat{\mathcal{H}}_{\text{phon-THz}} + \hat{\mathcal{H}}_{\text{exc-phon}} + \hat{\mathcal{H}}_{\text{laser}}, \quad (1)$$

where

$$\hat{\mathcal{H}}_{\text{exc-cavity}} = \sum_{\alpha=1,2}\sum_{\boldsymbol{k}_\parallel} \hbar\omega_x \hat{c}^\dagger_{\alpha,\boldsymbol{k}_\parallel}\hat{c}_{\alpha,\boldsymbol{k}_\parallel} + \hbar\omega_c(\boldsymbol{k}_\parallel,\delta)\hat{a}^\dagger_{\alpha,\boldsymbol{k}_\parallel}\hat{a}_{\alpha,\boldsymbol{k}_\parallel} + \hbar\Omega(\hat{a}^\dagger_{\alpha,\boldsymbol{k}_\parallel}\hat{c}_{\alpha,\boldsymbol{k}_\parallel} + \text{H.c.}) \quad (2)$$

describes the interaction between optical cavity photons (creation operator $\hat{a}^\dagger_{\alpha,\boldsymbol{k}_\parallel}$ for an in-plane momentum $\boldsymbol{k}_\parallel$ and a polarization state α) and a bright excitonic state (creation operator $\hat{c}^\dagger_{\alpha,\boldsymbol{k}_\parallel}$) in the strong-coupling regime; $2\hbar\Omega$ is the Rabi splitting between the upper and lower exciton-polariton states for zero detuning between the cavity and exciton. The energy of the excitonic transition does not depend on the wave vector and is given by $\hbar\omega_x = 1630$ meV in CdTe. We choose $\hbar\Omega = 6$ meV $< \hbar\omega_{\text{TO}}$, so that both phonon-polariton branches (lower and upper) can be used for the conversion mechanism. Such a Rabi splitting is easily achievable in CdTe microcavities [19].

Neglecting the dependency on the polarization [20], the cavity mode has the dispersion

$$\omega_c(\boldsymbol{k}_\parallel,\delta) = \omega_c^0 + \frac{\hbar|\boldsymbol{k}_\parallel|^2}{2m_{\text{eff}}} + \delta, \quad (3)$$

where $\omega_c^0 = ck_{z,0}/n_{\text{vis}}$ with $k_{z,0}$ fixed by the cavity length and $n_{\text{vis}} \simeq 2.5$ is the cavity medium refractive index in the visible range; $m_{\text{eff}} \simeq 10^{-5}m_e$ is the effective mass of the cavity photons, with m_e the free electron mass; δ is the cavity detuning. From now on, we take $\omega_c^0 = \omega_x$.

The interaction between TO phonons and THz photons in Eq. (1) has the form

$$\hat{\mathcal{H}}_{\text{phon-THz}} = \sum_{\boldsymbol{q}} \hbar\omega_{\text{TO}}\hat{b}^\dagger_{\boldsymbol{q}}\hat{b}_{\boldsymbol{q}} + \hbar\omega_{\text{ir}}(\boldsymbol{q})\hat{l}^\dagger_{\boldsymbol{q}}\hat{l}_{\boldsymbol{q}} + \hbar\Omega_{\text{ir}}(\hat{b}^\dagger_{\boldsymbol{q}}\hat{l}_{\boldsymbol{q}} + \hat{l}^\dagger_{\boldsymbol{q}}\hat{b}_{\boldsymbol{q}}), \quad (4)$$

where $\hat{b}^\dagger_{\boldsymbol{q}}$ creates a TO phonon with a three-dimensional momentum $\boldsymbol{q}$ and frequency ω_{TO} and $\hat{l}^\dagger_{\boldsymbol{q}}$ creates a THz photon with momentum $\boldsymbol{q}$ and dispersion

$$\omega_{\text{ir}}(\boldsymbol{q}) = (c/n_{\text{ir}})\sqrt{|\boldsymbol{q}_\parallel|^2 + q_z^2}, \quad (5)$$

where $n_{\text{ir}} = 3.57$ is the cavity medium refractive index in the THz range [21]. Phonons and THz photons are in strong

coupling, giving rise to phonon polaritons, with $2\hbar\Omega_{\rm ir} = 11.15$ meV being the phonon-polariton Rabi splitting [21].

The cornerstone of the conversion mechanism is the weak interaction between bright excitons and TO phonons, described by the optomechanical-like Hamiltonian [22]

$$\hat{\mathcal{H}}_{\text{exc-phon}} = -\sum_{\boldsymbol{q},\boldsymbol{k},\boldsymbol{k}'} \hbar g_{xb} (\hat{b}^{\dagger}_{-\boldsymbol{q},\text{TO}} + \hat{b}_{\boldsymbol{q},\text{TO}}) \delta_{\boldsymbol{q},\boldsymbol{k}-\boldsymbol{k}'} \times (\hat{c}^{\dagger}_{\boldsymbol{k},1} \hat{c}_{\boldsymbol{k}',2} + \hat{c}^{\dagger}_{\boldsymbol{k},2} \hat{c}_{\boldsymbol{k}',1}), \quad (6)$$

where $\boldsymbol{k}$, $\boldsymbol{k}'$, and $\boldsymbol{q}$ are three-dimensional wave vectors and $\alpha = 1, 2$ the exciton linear polarizations oriented along the crystalline axes $x = [010]$ and $y = [001]$. Notice that the exciton-phonon coupling is then diagonal in the basis where the linear polarizations are oriented at $\pm 45°$. This feature is in agreement with the results of Raman scattering theory, which involves the same interaction vertex [23]. The exciton-TO phonon interaction in zinc blende crystals occurs via the deformation potential. Owing to symmetries, the only nonvanishing matrix element are those coupling cross-polarized heavy-hole (*hh*) and light-hole (*lh*) exciton states [24,25], via the deformation potential in the direction perpendicular to the polarization plane (see [22]). Notice that, in order to involve both excitonic states with a comparable weight, it is important to use a bulk CdTe active layer inside the microcavity, while quantum wells would not be suitable, since the *hh* and *lh* exciton states are split by the confinement. The deformation potential has a nonzero matrix element, in the basis of cubic harmonics, e.g., $\langle X|V^{(z)}_{\rm DP}|Y\rangle$, where $V^{(z)}_{\rm DP}$ is the z component of the deformation potential vector (see [22]). Interestingly, this result agrees with the symmetry properties of the nonlinear susceptibility $\chi^{(2)}$ of zinc blende crystals in the spectral region we are interested in, whose only nonzero elements are d_{14}, d_{25}, and d_{36} following the standard nomenclature [26]. In particular, one may have $P_z = d_{36} E_x E_y$, i.e., a phonon polarization along z induced by applied fields in x and y directions thanks to the off-diagonal terms of the nonlinear susceptibility tensor. This is our case, since there is a preferential direction fixed by the cavity axis that fixes the incoming and outgoing photons to be polarized in the (x, y) plane. Correspondingly, the emitted phonons participating in the coupling to excitons are propagating in the cavity plane, i.e., $\mathbf{q} = (\mathbf{q}_{\parallel}, q_z = 0)$. The exciton-phonon coupling $\hbar g_{xb}$ that we obtain (see [22]) reads

$$\hbar g_{xb} = q_h \sqrt{\frac{\hbar M}{2\rho V \mu \omega_{\rm TO} a^2}} \frac{d_0}{2}, \quad (7)$$

where d_0 is the optical deformation potential [27,28], a is the length of the elementary cell of the lattice, ρ is the mass density of the semiconductor, V is the volume of the slab, and μ and M are the reduced and total mass, respectively, of the two ions of the elementary cell of the crystal. The prefactor q_h corresponds to the overlap between the orbitals describing the relative motion of electron and hole before and after the interaction of the exciton and the TO phonon. For a CdTe slab of size $V = 18\ \mu\text{m}^3$ using $d_0 = 30$ eV [29], we estimate $\hbar g_{xb} = 0.2\ \mu$eV [22].

Being orders of magnitude weaker as compared to Ω and $\Omega_{\rm ir}$, the interaction amplitude g_{xb} will be conveniently treated as a perturbation. Following Hopfield's transformation, we can rewrite $\hat{\mathcal{H}}_{\text{exc-cavity}}$ in the basis of upper and lower exciton polaritons [30]:

$$\begin{pmatrix} \hat{p}_{\alpha,\boldsymbol{k}} \\ \hat{u}_{\alpha,\boldsymbol{k}} \end{pmatrix} = \begin{pmatrix} -C_{\boldsymbol{k}} & X_{\boldsymbol{k}} \\ X_{\boldsymbol{k}} & C_{\boldsymbol{k}} \end{pmatrix} \begin{pmatrix} \hat{a}_{\alpha,\boldsymbol{k}} \\ \hat{c}_{\alpha,\boldsymbol{k}} \end{pmatrix}, \quad (8)$$

where $\hat{p}^{\dagger}_{\alpha,\boldsymbol{k}}$ and $\hat{u}^{\dagger}_{\alpha,\boldsymbol{k}}$ are the bosonic creation operator of the lower and upper exciton-polariton states, respectively, with in-plane momentum $\boldsymbol{k}$ and energy $\hbar\omega_{p,u}(\boldsymbol{k})$, where p (u) stands for the lower (upper) polariton. $C_{\boldsymbol{k}}$ and $X_{\boldsymbol{k}}$ are the usual Hopfield coefficients describing the photonic and excitonic fraction of these exciton-polariton states [41]. In the same way, we apply another Hopfield transformation [15] to the TO phonon or THz photon subspace that reads

$$\begin{pmatrix} \hat{w}_{\boldsymbol{q}} \\ \hat{z}_{\boldsymbol{q}} \end{pmatrix} = \begin{pmatrix} -N_{\boldsymbol{q}} & T_{\boldsymbol{q}} \\ T_{\boldsymbol{q}} & N_{\boldsymbol{q}} \end{pmatrix} \begin{pmatrix} \hat{b}_{\boldsymbol{q}} \\ \hat{l}_{\boldsymbol{q}} \end{pmatrix}, \quad (9)$$

where $\hat{w}^{\dagger}_{\boldsymbol{q}}$ and $\hat{z}^{\dagger}_{\boldsymbol{q}}$ are the bosonic creation operator of the lower and upper phonon-polariton states, respectively, with energy $\hbar\omega_w$ and $\hbar\omega_z$. $N_{\boldsymbol{q}}$ and $T_{\boldsymbol{q}}$ are the Hopfield coefficients describing the TO phonon and THz photon fraction, respectively, of these phonon-polariton states. In our total Hamiltonian, g_{xb} thus couples the exciton-polariton and phonon-polariton subspace; interestingly, since it is very weak as compared to the other coupling amplitudes $g_{xb} \ll \Omega, \Omega_{\rm ir}$, we can safely assume that the polaritonic states, whether excitons or phonons, remain the proper eigenstates of the system.

The last term in Eq. (1) describes the optical excitation that pumps the exciton-polariton states resonantly. We consider a two-pump scheme, as depicted in Fig. 1(b), which excites both the lower polariton branch of a given polarization, e.g., $\alpha = 1$, and the upper polariton branch of opposite polarization, i.e., $\alpha' = 2$ [42]. The pumps have amplitudes $\hbar\mathcal{R}_{\pm}$, wave vector $\boldsymbol{k}_{\pm}$, and frequency $\omega_{\pm}$. The corresponding Hamiltonian reads

$$\hat{\mathcal{H}}_{\text{laser}} = \hbar\mathcal{R}_{-} e^{-i\omega_{-}t} \hat{p}^{\dagger}_{1,\boldsymbol{k}_{-}} + \hbar\mathcal{R}_{+} e^{-i\omega_{+}t} \hat{u}^{\dagger}_{2,\boldsymbol{k}_{+}} + \text{H.c.} \quad (10)$$

In the following, we focus on the two exciton-polariton states which are macroscopically populated by the laser pump, i.e., $\hat{p}_1$ and $\hat{u}_2$. Among the various exciton-phonon interaction terms in $\hat{\mathcal{H}}_{\text{exc-phon}}$ generated by the Hopfield transformations (8) and (9), we keep those which describe the frequency-conversion process we are interested in, namely, $\hat{p}^{\dagger}_1 \hat{u}_2 \hat{w}^{\dagger}$ and $\hat{p}^{\dagger}_1 \hat{u}_2 \hat{z}^{\dagger}$. These processes are summarized in the diagrams in Fig. 1(c).

In order to determine the input-output characteristics of the system in the steady state, accounting for the thermal

noise contribution, we derive the corresponding Heisenberg-Langevin equations

$$\dot{\hat{p}}_{1,\boldsymbol{k}_-} = -i\omega_p(\boldsymbol{k}_-)\hat{p}_{1,\boldsymbol{k}_-} + ig_{xb}X_{\boldsymbol{k}_-}C_{\boldsymbol{k}_+}\hat{u}_{2,\boldsymbol{k}_+}(-N_{-\boldsymbol{q}}\hat{w}^\dagger_{-\boldsymbol{q}} + T_{-\boldsymbol{q}}\hat{z}^\dagger_{-\boldsymbol{q}}) - i\mathcal{R}_-e^{-i\omega_- t} - \gamma_p\hat{p}_{1,\boldsymbol{k}_-} + \sqrt{2\gamma_p}\hat{p}_{1,\mathrm{in}}(t), \quad (11)$$

$$\dot{\hat{u}}_{2,\boldsymbol{k}_+} = -i\omega_u(\boldsymbol{k}_+)\hat{u}_{2,\boldsymbol{k}_+} + ig_{xb}C_{\boldsymbol{k}_+}X_{\boldsymbol{k}_-}\hat{p}_{1,\boldsymbol{k}_-}(-N_{\boldsymbol{q}}\hat{w}_{\boldsymbol{q}} + T_{\boldsymbol{q}}\hat{z}_{\boldsymbol{q}}) - i\mathcal{R}_+e^{-i\omega_+ t} - \gamma_u\hat{u}_{2,\boldsymbol{k}_+} + \sqrt{2\gamma_u}\hat{u}_{2,\mathrm{in}}(t), \quad (12)$$

$$\dot{\hat{w}}_{\boldsymbol{q}} = -i\omega_w(\boldsymbol{q})\hat{w}_{\boldsymbol{q}} - ig_{xb}N_{\boldsymbol{q}}X_{\boldsymbol{k}_-}C_{\boldsymbol{k}_+}\hat{p}^\dagger_{1,\boldsymbol{k}_-}\hat{u}_{2,\boldsymbol{k}_+} - \gamma_w\hat{w}_{\boldsymbol{q}} + \sqrt{2\gamma_w}\hat{w}_{\mathrm{in}}(t), \quad (13)$$

$$\dot{\hat{z}}_{\boldsymbol{q}} = -i\omega_z(\boldsymbol{q})\hat{z}_{\boldsymbol{q}} + ig_{xb}T_{\boldsymbol{q}}X_{\boldsymbol{k}_-}C_{\boldsymbol{k}_+}\hat{p}^\dagger_{1,\boldsymbol{k}_-}\hat{u}_{2,\boldsymbol{k}_+} - \gamma_z\hat{z}_{\boldsymbol{q}} + \sqrt{2\gamma_z}\hat{z}_{\mathrm{in}}(t), \quad (14)$$

where the condition $\boldsymbol{q} = \boldsymbol{k}_+ - \boldsymbol{k}_-$ is assumed all through Eqs. (11)–(14), $\gamma_{p,u,w,z}$ are the decay rates of exciton polaritons and photon polaritons, and $\hat{\zeta}_{\mathrm{in}} = \hat{p}_{\mathrm{in}}, \hat{u}_{\mathrm{in}}, \hat{w}_{\mathrm{in}}, \hat{z}_{\mathrm{in}}$ are input noise fields, with $\langle\hat{\zeta}_{\mathrm{in}}(t)\rangle = 0$ and $\langle[\hat{\zeta}_{\mathrm{in}}(t), \hat{\zeta}^\dagger_{\mathrm{in}}(t')]\rangle = \delta(t-t')$ [43]. The decay rates of upper and lower exciton polaritons can be estimated using excitonic γ_x and photonic κ decay rates according to $\gamma_u = \gamma_x C^2_{\boldsymbol{k}_+} + \kappa X^2_{\boldsymbol{k}_+}$ and $\gamma_p = \gamma_x X^2_{\boldsymbol{k}_-} + \kappa C^2_{\boldsymbol{k}_-}$. Correspondingly, we use $\gamma_w = \gamma_b N^2_{\boldsymbol{q}} + \gamma_l T^2_{\boldsymbol{q}}$ and $\gamma_z = \gamma_b T^2_{\boldsymbol{q}} + \gamma_l N^2_{\boldsymbol{q}}$ for the decay rates of the lower and upper phonon polariton, respectively. At room temperature, the only non-negligible noise is the one originating from phonons and THz photons, populated according to $\bar{n}_b = [1/(e^{\hbar\omega_{\mathrm{TO}}/k_BT} - 1)]$ and $\bar{n}_l = [1/(e^{\hbar\omega_{\mathrm{ir}}/k_BT} - 1)]$, respectively. Since $g_{xb} \ll \Omega, \Omega_{\mathrm{ir}}$, we can decouple the Heisenberg-Langevin equations (11)–14)). We first obtain the expectation value of $\hat{p}^\dagger_{1,\boldsymbol{k}_-}\hat{u}_{2,\boldsymbol{k}_+}$ for times longer than the characteristic time scale of the Rabi oscillations ($t \gg T_R = 1/\tilde{\Omega}$), corresponding to $n_0(t) \equiv \langle\hat{p}^\dagger_{1,\boldsymbol{k}_-}(t)\hat{u}_{2,\boldsymbol{k}_+}(t)\rangle_{t\gg T_R}$, from Eqs. (11) and (12) assuming $g_{xb} \simeq 0$ and neglecting correlations. Pumping both exciton-polariton branches leads to an effective pumping of the phonon-polariton branches at frequency $\tilde{\Omega} = \omega_+ - \omega_-$. This frequency-difference generation scheme follows from the specific nonlinearity of the exciton-phonon coupling Eq. (6). Inserting the solution for $n_0(t)$ in Eqs. (13) and (14), we find the number of phonon polaritons in lower and upper modes $N_w = \langle w^\dagger_{\boldsymbol{q}}(t)w_{\boldsymbol{q}}(t)\rangle$ and $N_z = \langle z^\dagger_{\boldsymbol{q}}(t)z_{\boldsymbol{q}}(t)\rangle$ at large times $t \gg T_R$:

$$N_w = \frac{|\tilde{\mathcal{R}}|^2N^2(\boldsymbol{q})}{\gamma_w^2 + [\tilde{\Omega} - \omega_w(\boldsymbol{q})]^2} + \frac{\gamma_b}{\gamma_w}N^2(\boldsymbol{q})\bar{n}_b(\omega_{\mathrm{TO}}) + \frac{\gamma_l}{\gamma_w}T^2(\boldsymbol{q})\bar{n}_l(\omega_{\mathrm{ir}}), \quad (15)$$

$$N_z = \frac{|\tilde{\mathcal{R}}|^2T^2(\boldsymbol{q})}{\gamma_z^2 + [\tilde{\Omega} - \omega_z(\boldsymbol{q})]^2} + \frac{\gamma_b}{\gamma_z}T^2(\boldsymbol{q})\bar{n}_b(\omega_{\mathrm{TO}}) + \frac{\gamma_l}{\gamma_z}N^2(\boldsymbol{q})\bar{n}_l(\omega_{\mathrm{ir}}), \quad (16)$$

with effective pump strength

$$\tilde{\mathcal{R}} = \frac{g_{xb}X_{\boldsymbol{k}_-}C_{\boldsymbol{k}_+}\mathcal{R}^*_-\mathcal{R}_+}{[-i\gamma_p - (\omega_p - \omega_-)][i\gamma_u - (\omega_u - \omega_+)]}. \quad (17)$$

Equations (15)–(17) show that our frequency-difference generation scheme is based on a triple resonance, yielding a giant effective $\chi^{(2)} = 1035$ pm/V for the intracavity fields (see [22]). Owing to the triple resonance conditions, this value is 10 times larger than that found in other materials used for difference frequency generation of THz light [44,45]. Note that for fields considered outside the cavity $\chi^{(2)}$ is even much larger, i.e., by a typical factor $\propto X_{\boldsymbol{k}_-}C_{\boldsymbol{k}_+}Q$, where Q is the bare cavity quality factor. $Q \simeq 2000$ is routinely achieved in CdTe microcavities [19].

The emission power of THz photons, i.e., the photonic fraction of lower and upper phonon polaritons, is given by $P_{\mathrm{out}} = T^2N_w\gamma_w\hbar\omega_w + N^2N_z\gamma_z\hbar\omega_z$. Figure 2 shows the power conversion efficiency $\eta = P_{\mathrm{out}}/(P^+_{\mathrm{in}}P^-_{\mathrm{in}})$, as a function of frequency $\tilde{\Omega}$ and the in-plane wave vector for resonant pumping, the input power of each pump being $P^\pm_{\mathrm{in}} = \hbar\omega_\pm[(2|\mathcal{R}_\pm|^2)/(|\Lambda_\pm|^2\gamma_{p,u})]$ with $\Lambda_+ = X_{\boldsymbol{k}_+}$ and $\Lambda_- = C_{\boldsymbol{k}_-}$. Thanks to the triple resonance condition, we find a very large efficiency as compared to existing frequency-difference generation schemes for THz emission,

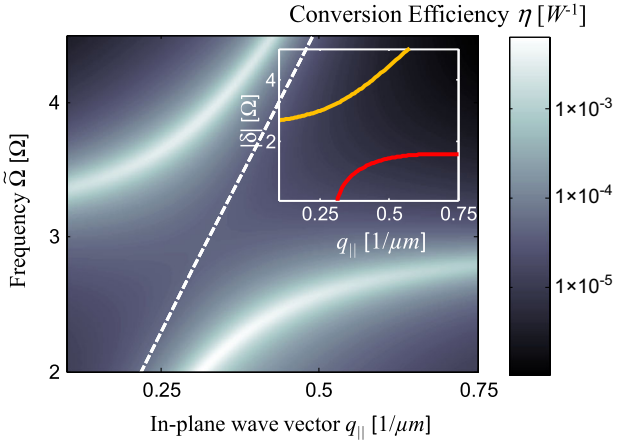

FIG. 2. Power conversion efficiency of THz photons (in the logarithmic scale) as a function of frequency $\tilde{\Omega}$ (in units of Ω) and in-plane wave vector $q_\parallel = |\boldsymbol{q}_\parallel|$ (in units of $\mu\mathrm{m}^{-1}$) for resonant pumping $\omega_- = \omega_p$ and $\omega_+ = \omega_u$. We take $\kappa = 0.1$ THz, $\gamma_b = 0.35$ THz, $\gamma_l = 0.6$ THz, and $\gamma_w = \gamma_z \simeq 0.6$ THz [21], assuming for simplicity a momentum-independent value. The decay rate of the exciton is neglected, since $\gamma_x \sim 0.01$ THz. The white dashed line is the light cone $\omega_{\mathrm{ir}}(q_\parallel) = (c/n_{\mathrm{ir}})|\boldsymbol{q}_\parallel|$. Inset: Cavity detuning $|\delta|$ in units of Ω as a function of $q_\parallel$ for $\tilde{\Omega} = \omega_w$ (red curve) and $\tilde{\Omega} = \omega_z$ (yellow curve).

e.g., 10 times larger than in graphene pumped at telecom frequencies [46] and orders of magnitude larger than infrared wavelength converters [47].

One main advantage of the proposed scheme is that the THz frequency $\tilde{\Omega}$ is easily tunable in actual experiments: Its lowest value is fixed by the Rabi splitting Ω; it depends both on the wave vector $q_\parallel$ and on the detuning δ between the cavity and exciton in Eq. (3), adjustable using the microcavity intentional wedged shape [41]. For $\tilde{\Omega}$ matching the frequency of the upper or lower phonon-polariton branch, δ depends on the wave vector $q_\parallel$ (inset in Fig. 2).

As explained above, the THz emission takes place in the plane of the microcavity with a wave vector $\mathbf{q}_\parallel$. In order to collect easily this emission, the simplest strategy is to etch or deposit microstructures on the cavity surface, such as a grating or so-called "bulls-eyes" [48], in order to scatter the THz photons back into the forward direction. The typical pitch of such structures has to be comparable and larger than the THz wavelength, i.e., $\sim 50\ \mu$m, which poses no technological difficulty.

In conclusion, we have presented a frequency down-conversion scheme to convert optical photons in THz photons in a CdTe semiconductor microcavity. The scheme is based on an engineered $\chi^{(2)}$ optical nonlinearity coming from the weak interaction between bright excitons and TO phonons and does not involve any change in the microcavity material nor an externally applied field. For future applications, the case of large band gap material is promising in two respects: (i) the strong-coupling regime is stable at room temperature, with obvious benefits for the future realization of an actual polaritonic THz devices, and (ii) the TO phonon energy [$\hbar\omega_{\mathrm{TO}} = (66.5; 69.5)$ meV in GaN and $\hbar\omega_{\mathrm{TO}} = (47.7; 51.7)$ meV in ZnO [49]] can be well matched by the Rabi splitting in a state-of-the-art microcavity [50–52]. Because of their wurtzite crystalline structure, additional calculations are needed to determine exactly the value of the bright exciton TO phonon coupling strength, but symmetry considerations suggest that our mechanism should be applicable as well.

The authors acknowledge discussions with Joël Cibert. This work is supported by French state funds ANR-10-LABX-51-01 (Labex LANEF du Programme d'Investissements d'Avenir) and ANR-16-CE30-0021 (QFL), the French-German University (UFA/DFH), the German Research Foundation (DFG: "DACH: Quantum crystals of matter and light", BI 1694), and the German Ministry of Education and Research (BMBF "Qu.com").

*anna.minguzzi@lpmmc.cnrs.fr

[1] J. F. Federici, B. Schulkin, F. Huang, D. Gary, R. Barat, F. Oliveira, and D. Zimdars, Semicond. Sci. Technol. **20**, S266 (2005).
[2] M. Tonouchi, Nat. Photonics **1**, 97 (2007).
[3] R. A. Lewis, J. Phys. D **47**, 374001 (2014).
[4] C. Weisbuch, M. Nishioka, A. Ishikawa, and Y. Arakawa, Phys. Rev. Lett. **69**, 3314 (1992).
[5] Y. Hokomoto, Y. Kadoya, and M. Yamanishi, Appl. Phys. Lett. **74**, 3839 (1999).
[6] A. V. Kavokin, I. A. Shelykh, T. Taylor, and M. M. Glazov, Phys. Rev. Lett. **108**, 197401 (2012).
[7] M. A. Kaliteevski, K. A. Ivanov, G. Pozina, and A. J. Gallant, Sci. Rep. **4**, 5444 (2014).
[8] S. Huppert, O. Lafont, E. Baudin, J. Tignon, and R. Ferreira, Phys. Rev. B **90**, 241302(R) (2014).
[9] S. De Liberato, C. Ciuti, and C. C. Phillips, Phys. Rev. B **87**, 241304 (2013).
[10] S. A. Holmstrom, T. H. Stievater, M. W. Pruessner, D. Park, W. S. Rabinovich, J. B. Khurgin, C. J. K. Richardson, S. Kanakaraju, L. C. Calhoun, and R. Ghodssi, Phys. Rev. B **86**, 165120 (2012).
[11] F. Barachati, S. De Liberato, and S. Kéna-Cohen, Phys. Rev. A **92**, 033828 (2015).
[12] I. Carusotto and C. Ciuti, Rev. Mod. Phys. **85**, 299 (2013).
[13] J. Kasprzak, D. D. Solnyshkov, R. André, L. S. Dang, and G. Malpuech, Phys. Rev. Lett. **101**, 146404 (2008).
[14] M.Saba, C. Ciuti, J. Bloch, V. Thierry-Mieg, R. André, L. S. Dang, S. Kundermann, A. Mura, G. Bongiovanni, J. L. Staehli, and B. Deveaud, Nature (London) **414**, 731 (2001).
[15] C. H. Henry and J. J. Hopfield, Phys. Rev. Lett. **15**, 964 (1965).
[16] J. Bochmann, A. Vainsencher, D. D. Awschalom, and A. N. Cleland, Nat. Phys. **9**, 712 (2013).
[17] R. W. Andrews, R. W. Peterson, T. P. Purdy, K. Cicak, R. W. Simmonds, C. A. Regal, and K. Lehnert, Nat. Phys. **10**, 321 (2014).
[18] T. Bagci, A. Simonsen, S. Schmid, L. G. Villanueva, E. Zeuthen, J. Appel, J. M. Taylor, A. Sorensen, K. Usami, A. Schliesser, and E. S. Polzik, Nature (London) **507**, 81 (2014).
[19] M. Richard, J. Kasprzak, R. Romestain, R. André, and L. S. Dang, Phys. Rev. Lett. **94**, 187401 (2005).
[20] G. Panzarini, L. C. Andreani, A. Armitage, D. Baxter, M. S. Skolnick, V. N. Astratov, J. S. Roberts, A. V. Kavokin, M. R. Vladimirova, and M. A. Kaliteevski, Phys. Rev. B **59**, 5082 (1999).
[21] M. Schall, M. Walther, and P. U. Jepsen, Phys. Rev. B **64**, 094301 (2001).
[22] See Supplemental Material at http://link.aps.org/supplemental/10.1103/PhysRevLett.119.127401 for details, which includes Refs. [21,23–40].
[23] M. Cardona and P. Y. Yu, *Fundamentals of Semiconductors Physics and Materials Properties* (Springer, Berlin, 2010).
[24] A. Cantarero, C. Trallero-Giner, and M. Cardona, Phys. Rev. B **39**, 8388 (1989).
[25] A. Ganguly and J. Birman, Phys. Rev. **162**, 806 (1967).
[26] R. W. Boyd, *Nonlinear Optics* (Academic, London, 2008).
[27] G. L. Bir and G. E. Pikus, Fiz. Tverd. Tela (Leningrad) **2**, 2287 (1960).
[28] G. L. Bir and G. E. Pikus, *Symmetry and Strain-Induced Effects in Semiconductors* (Wiley, New York, 1974).
[29] W. Pötz and P. Vogl, Phys. Rev. B **24**, 2025 (1981).
[30] J. J. Hopfield, Phys. Rev. **112**, 1555 (1958).

[31] O. Madelung, *Introduction to Solid-State Theory* (Springer, Berlin, 1978).
[32] R. Scholz, J. Appl. Phys. **77**, 3219 (1995).
[33] Y. Toyozawa, Prog. Theor. Phys. **20**, 53 (1958).
[34] R. Knox, *Theory of Excitons* (Academic, New York, 1963).
[35] G. Wannier, Phys. Rev. **52**, 191 (1937).
[36] J. Luttinger and W. Kohn, Phys. Rev. **97**, 869 (1955).
[37] F. Bassani and G. P. Parravicini, *Electronic States and Optical Transitions in Solids* (Pergamon, Oxford, 1975).
[38] A. Rubio-Ponce, D. Olguín, and I. Hernández-Calderón, Superficies Vacio **16**, 26 (2003).
[39] V. Savona, C. Piermarocchi, A. Quattropani, P. Schwendimann, and F. Tassone, Phase Transitions **68**, 169 (1999).
[40] R. André, D. Heger, L. S. Dang, and Y. M. d'Aubigné, J. Cryst. Growth **184**, 758 (1998).
[41] *The Physics of Semiconductor Microcavities*, edited by B. Deveaud (Wiley, Weinheim, 2007).
[42] As an alternative, one may use the same polarization direction for the two pumps, oriented at 45° with respect to the x, y plane.
[43] C. W. Gardiner and M. J. Collett, Phys. Rev. A **31**, 3761 (1985).
[44] S. Y. Tochitsky, C. Sung, S. E. Trubnick, C. Joshi, and K. L. Vodopyanov, J. Opt. Soc. Am. B **24**, 2509 (2007).
[45] E. B. Petersen, W. Shi, A. Chavez-Pirson, N. Peyghambarian, and A. T. Cooney, Appl. Phys. Lett. **98**, 121119 (2011).
[46] X. Yao, M. Tokman, and A. Belyanin, Phys. Rev. Lett. **112**, 055501 (2014).
[47] M. Cazzanelli, F. Bianco, E. Borga, G. Pucker, M. Ghulinyan, E. Degoli, E. Luppi, V. Véniard, S. Ossicini, D. Modotto, S. Wabnitz, R. Pierobon, and L. Pavesi, Nat. Mater. **11**, 148 (2011).
[48] L. Sapienza, M. Davanço, A. Badolato, and K. Srinivasan, Nat. Commun. **6**, 7833 (2015).
[49] The first (second) number in the parentheses corresponds to a TO phonon mode polarized parallel (perpendicular) to the wurtzite's C axis.
[50] F. Li, L. Orosz, O. Kamoun, S. Bouchoule, C. Brimont, P. Disseix, T. Guillet, X. Lafosse, M. Leroux, J. Leymarie, M. Mexis, M. Mihailovic, G. Patriarche, F. Réveret, D. Solnyshkov, J. Zuniga-Perez, and G. Malpuech, Phys. Rev. Lett. **110**, 196406 (2013).
[51] A. Trichet, L. Sun, G. Pavlovic, N. A. Gippius, G. Malpuech, W. Xie, Z. Chen, M. Richard, and L. S. Dang, Phys. Rev. B **83**, 041302 (2011).
[52] G. Christmann, R. Butté, E. Feltin, A. Mouti, P. A. Stadelmann, A. Castiglia, J. F. Carlin, and N. Grandjean, Phys. Rev. B **77**, 085310 (2008).